NJC

Accepted Manuscript

This is an *Accepted Manuscript*, which has been through the Royal Society of Chemistry peer review process and has been accepted for publication.

Accepted Manuscripts are published online shortly after acceptance, before technical editing, formatting and proof reading. Using this free service, authors can make their results available to the community, in citable form, before we publish the edited article. We will replace this *Accepted Manuscript* with the edited and formatted *Advance Article* as soon as it is available.

You can find more information about *Accepted Manuscripts* in the Information for Authors.

Please note that technical editing may introduce minor changes to the text and/or graphics, which may alter content. The journal's standard Terms & Conditions and the Ethical guidelines still apply. In no event shall the Royal Society of Chemistry be held responsible for any errors or omissions in this *Accepted Manuscript* or any consequences arising from the use of any information it contains.

ROYAL SOCIETY OF CHEMISTRY

www.rsc.org/njc

Title: Conducting Poly (o-anisidine) nanofibres dispersed epoxy–siloxane composite coatings: synthesis, characterization and corrosion protective performance

Names of Authors

Neha Kanwar Rawat

Research scholar

Materials Research Laboratory, Dept of Chemistry

Jamia Millia Islamia, New Delhi. 110025.

Email: neharawatjmi@gmail.com

Dr. Shabnam Pathan

Materials Research Laboratory, Dept of Chemistry

Jamia Millia Islamia, New Delhi. 110025.

Email:saimachm@gmail.com

Dr. Alok Kumar Sinha

Scientist E

Department of Science and Technology

New Delhi

Email: alokkumar.sinha@nic.in

*Prof. Sharif Ahmad

Materials Research Laboratory, Dept of Chemistry

Jamia Millia Islamia, New Delhi. 110025.

Email: sharifahmad_jmi@yahoo.co.in

***Corresponding Author**

Tel. no. +91 11 26827508

Fax: +91 11 26840229

Conducting Poly (o-anisidine) nanofibres dispersed epoxy–siloxane composite coatings: synthesis, characterization and corrosion protective performance

Neha Kanwar Rawat[a], Dr. Shabnam Pathan[a], Dr. Alok Kumar Sinha[b] and *Prof. Sharif Ahmad[a]

a Materials Research Laboratory, Dept of Chemistry

Jamia Millia Islamia, New Delhi. 110025

b Department of Science and Technology

New Delhi

Abstract

Conducting polymers (CPs) have exhibited a promising ability for corrosion inhibition and find application in the formulation of new generation smart anti-corrosive coating materials. CPs not only acts as an active barrier for corrosive ions but also provide protection to the metal substrate through redox mechanism. In view of this, the present article reports the synthesis, structural, physico-chemical, physico-mechanical characterization and corrosion protective performance of tartaric acid (TA) and a functionalized protonic acid-dodecyl benzenesulphonic acid (DBSA) doped poly(o-anisidine) nanoparticles (TA-DBSA-POA) and these nanoparticles dispersed epoxy-siloxane (ES) nanocomposites coatings (TA-DBSA-POA-ES) on carbon steel (CS). The structure, size and morphology of TA-DBSA-POA nanoparticles and that of coatings were investigated by FT-IR, XRD, TEM and SEM analysis. The conductivity of TA-DBSA-POA nanoparticles (2.09 S/cm), and TA-DBSA-POA-ES nanocomposites (5.02E-3 S/cm) as well as their thermal stability were investigated with the help of four-probe and TGA technique. The physico-mechanical properties of these coatings were evaluated by standard laboratory methods. To the best of our knowledge, the corrosion protective performance of these coatings was investigated for the first time in our laboratory, using salt spray test (SST), potentiodynamic polarization (PDP), and electron

impedance spectroscopy (EIS) techniques in varying concentration of NaCl viz 3.5 wt.%, 5.0 wt.% and 7.0 wt.% NaCl. SEM-EDAX and Raman studies revealed the presence of passive ferric oxide layer. These studies revealed that the nanocomposite coatings have shown far superior thermal stability, physico-mechanical and corrosion protective performance than those of plain ES and other such CPs reinforced epoxy coating systems.

Keywords: Poly(o-anisidine); Hydrogen bonding; Corrosion; Doping; Nanocomposites, Electron impedance spectroscopy

1. INTRODUCTION

Corrosion poses a serious economic and industrial threat as well as latent danger to humans. Further, it is important to mention that the corrosion cannot be prevented but can be control through different strategies, which retards the corrosion kinetics by altering its mechanism using cathodic protection, protective coatings and corrosion inhibitors or combination thereof [1-4]. In recent years nano conducting [5] polymers (Cps) have not only been used as corrosion inhibitors but also as fillers in doped and undoped state [6] in polymer nanocomposite coatings. The nano conducting polymer composite coatings have exhibited very promising physico-mechanical and thermal resistant anti-corrosive properties, which has helped in the processing of new generation smart coatings materials. These coatings sometimes also act as a good corrosion sensors for inhibition [7].

Generally, chromium passivation techniques were used for the pre-treatment of metal surface to enhance the adhesion between polymer coatings and metal surface, which can be correlated to its strong oxidative nature in hexavalent state that provide extra corrosion inhibition ability to coatings. However, because of highly toxic nature, hexachromate has been worldwide banned by the act of environmental legislation [8]. Thus, there is an urgent need to develop some green alternative surface pre-treatment technique to replace the present

carcinogenic hexavalent passivation technique. Literature revealed that in the field of corrosion protection CPs act as a green [9, 10] primers, e.g. PANI and its various derivatives like poly (o-anisidine) could acts as promising alternatives to the chromate passivation techniques owing to its ease of synthesis, availability, cost effectiveness and stability[11, 12]. The doping of CPs with organic acids reasonably improved properties like stability [13], solubility and conductivity [5, 14, 15]. Literature, also reports that the doped POA nanoparticles have exhibited enhanced mechanical stability with low percolation threshold and high conductivity as compared that of undoped conventional POA. PANI doped para-toluenesulphonic acid-DGEBA nanocomposites showed good thermomechanical and dielectric properties [16]. Similarly, Tartaric acid doped PANI had exhibited enhanced spectral, thermal, optical and conducting properties [17]. Interestingly, in addition to this a number of studies on PANI and its derivatives with their reference to their corrosion inhibition activity have also been reported [1, 2, 8, 11, 18-25]. However, there is no report available on the effect of two coupled dopants i.e organic surfactant-acid dopants on synthesis, physico-mechanical and anti-corrosion protection properties of poly (o-anisidine) nanoparticles dispersed epoxy–siloxane nanocomposite coatings.

Among the conventional polymers, epoxy resins find extensive industrial applications due to their low shrinkage, ease of cure, processing, higher adhesion strength, excellent moisture, solvent and chemical resistance [2, 20, 26-37]. However, the shortcomings in epoxy prevails such as low fracture energy, low pigment holding ability, poor hydrophobicity weathering resistance, discolouration on UV exposure and poor impact strength, which limit their application as a topcoat material in the field of paints and coatings. The use of modifiers, as second component in the epoxy has helped in combating these shortcomings. Silicone in epoxy is considered as best among various modifiers like rubber, clay, fibres etc. In order to improve further, the addition of hydroxyl terminated poly(dimethylsiloxane) (HPDMS) in

epoxy-siloxane blend further improved the properties as per our reported earlier method [27]. Secondly, it has been reported, that the dispersion of nanoCPs fillers [10, 14, 38] in epoxy matrix lead to the formation of nanocomposite which have, tailored properties and improve all the above cited shortcomings of neat epoxy matrix.

In view of this, the present article reports the synthesis of bi-dopant (TA and DBSA) doped POA nanoparticles and their dispersed epoxy siloxane (ES) nanocomposite coatings, their spectral, physic-mechanical and electrochemical corrosion characterization were also reported. To the best of our knowledge these studies have not been reported till date. The corrosion resistance performances of these coatings were investigated by potentiodynamic, electrochemical impedance spectroscopy and salt spray techniques. These studies revealed that the nanocomposite coatings showed superior corrosion protective performance as compared to plain ES and other conducting nanocomposite coatings[11, 20, 24, 39, 40].

2. EXPERIMENTAL

2.1. Materials

Ortho-anisidine monomer (M.W 123.16 g/mol and density 1.0923 g/cm^3) (Merck, Germany) was distilled twice under reduced pressure and stored in a refrigerator prior to use, Epoxy (DGEBA, D.E.R 332, epoxy equivalent 180–185, sp.gr. 1.2306, refractive index 1.5685, viscosity about 10,000 CP) DOW Chemicals, dodecylbenzenesulphonic acid (DBSA), phosphoric acid, Ammonium peroxydisulphate (APS) (S.D fine chem., India), tartaric acid (M.W 150.087, density 1.7 g/ml) , ethyl methyl ketone, Hydroxyl-terminated poly(dimethyl siloxane) (HPDMS,) (viscosity 90-150 cSt , refractive index 1.4057, density 0.970 g/cm^3 at 25° C) and hydrochloric acid (HCl) (Sigma-Aldrich, USA) were used as received.

2.2 Synthesis of TA-DBSA-POA nanoparticles

TA-DBSA doped POA nanoparticles were synthesized using in-situ emulsion polymerization technique. The freshly double distilled o-anisidine monomer (1.0g) and tartaric acid (0.2g) were injected to the reaction flask having DBSA (0.5 g) in 100 ml of 0.1 M HCl solution under constant stirring. The APS (as initiator) solution was prepared in 10 ml of 0.1 M HCl and added dropwise to the reaction mixture at room temperature. The total volume of the solution was maintained upto 110 ml. The reaction mixture was continuously stirred at 20-25 ^{o}C (as the Kraft temperature of DBSA is known around 15 ^{o}C) on mechanical stirrer for 14 h. The brownish colour residue of tartaric acid doped POA was filtered and washed several times with methanol, and dried in vacuum oven at 50 ^{o}C for 2 days resulting in the formation of brown colour precipitates as per the Fig.1. The yield of TA-DBSA-POA nanoparticles was found to be 65 %, comparable with those of earlier studies of POA synthesis. The successful formation of TA-DBSA-POA nanoparticles was confirmed by FT-IR analysis.

2.3 Synthesis of TA-DBSA-POA-ES nanocomposite coating formulations

ES was synthesized as per our earlier reported method [27]. DGEBA resin was pre activated at 120 ^{o}C for 30 min. The 4:1 ratio of pre-activated DGEBA and HPDMS was taken in three necked flat bottom flask fitted with magnetic stirrer, thermometer and nitrogen inlet. The 0.02g of phosphoric acid act as catalyst was added in a reaction mixture. The reaction mixture was continuously stirred on magnetic stirrer at 80 ^{o}C, for 45 min. The reaction between DGEBA and HPDMS took place by SN^2 mechanism and thus resulted in the formation of highly crosslinked ES network structure.

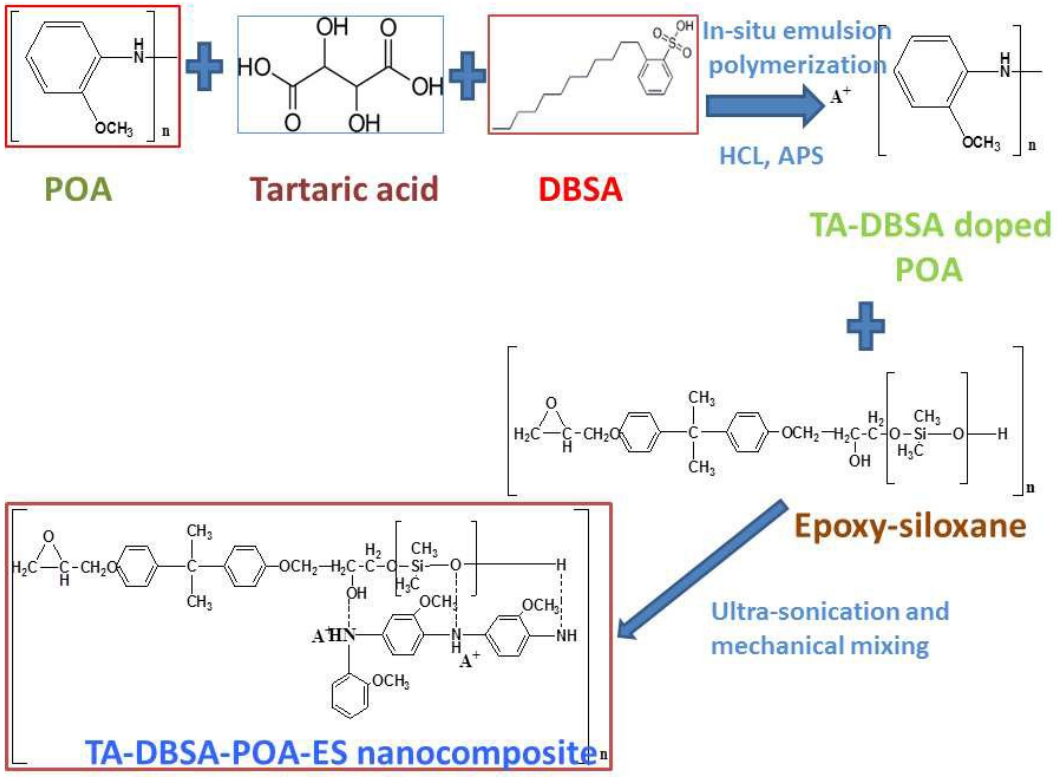

Fig. 1 Scheme for the formulation of TA-DBSA-POA-ES nanocomposite where A represents dopants

Then, different wt.% of synthesised TA-DBSA-POA nanoparticles (0.5, 1 and 1.5 % by weight) was dispersed in 10.0 g of ES matrix through sonication, using ultrasonic wave sonicator at 30 ˚C for a period of 30 min followed by mechanical stirring for 5 h at room temperature, resulted in the formation of homogeneously dispersed solution of TA-DBSA-POA-ES nanocomposite. The nanocomposite solution was kept under observation for fortnight to see whether any separation, occurred or not. However, no separation was observed. TA-DBSA-POA nanoparticle loading in ES showed uniform dispersion upto 1.5 wt. % however, beyond this loading agglomeration and phase separation was appeared. The coatings of nanoparticles dispersed TA-DBSA-POA solutions were prepared and applied by brush technique on the finally polished and degreased surface of CS specimen of standard

sizes. The coatings get cured within 30 min at room temperature and are formed with an average thickness of 120 μm.

2.4. Characterization

Fourier transform infrared (FT-IR) spectra of TA-DBSA-POA, ES matrix and TA-DBSA-POA-ES nanocomposites were taken on a PerkinElmer 1750 FT-IR spectrophotometer (PerkinElmer Instruments, Norwalk, CT) in the form of KBr pellets or with the help of NaCl cell. The particle sizes and its surface morphology analysis was demonstrated with the help of Transmission electron microscopy (TEM) model Morgagni 268-D TEM, FEI, USA operated at an accelerated voltage of 120 kV and Scanning electron microscopy on Scanning Electron Microscope model FEI Quanta 200F with Oxford-EDS system IE 250 X Max 80. The crystalline nature and phase purity were demonstrated on Philips X-ray diffractometer model Philips W3710 using CuKα radiation. Thermo gravimetric analysis (TGA) was performed using the SII EXSTAR 6000 thermal analyzer (Japan) in the range 40 ^{o}C to 800 ^{o}C under nitrogen gas environment at a flow rate of 10^{o} C/min. The specific gravity, epoxy equivalent, inherent viscosity and refractive index of these composite solutions were measured with the help of standard ASTM methods. The coatings of ES and TA-DBSA-POA-ES composite were prepared with the help of brush technique on the surface of 70×30×1 mm size CS strips for the preparation of coatings for the determination of their specular gloss at 45 ^{o} by a gloss meter (model RSPT-20, digital instrument Santa Barbara, CA), scratch hardness (BS 3900), bend test on 1/8" inch conical mandrel (ASTM D 3281-04) and impact resistance (IS: 101 par 5/sec-31988). For each test, five samples were used and their average values were determined using error bars representing standard deviation. The conductivity was measured by the standard four probe method using a Keithley DMM 2001 and EG and G Princeton Applied Research potentiostat model 362 as a current source. For each composite, three specimens were used for the measurement of conductivity. The mean values of the

conductivity were taken. Corrosion resistance performance of the ES and TA-DBSA-POA-ES coated CS strips specimens were evaluated by potentiodynamic polarization in different wt. % of NaCl (3.5, 5.0 and 7.0 wt %) at room temperature (30^0C) using micro Autolab type III with FRA unit (μ3AVT 70762, Netherlands) potentiostat. The Tafel plots in presence of these corrosive medium were obtained using a three-electrode electrochemical cell (EG&G 362) containing platinum gauze as counter electrode, Ag/AgCl as reference and test specimen (coated and uncoated mild steel specimens) as working electrodes. The 1.0 cm^2 area of working electrode was exposed to the solution. Prior to potentiodynamic polarization and EIS test, working electrode was allowed to stabilize for 20 min and then its open circuit potential (OCP) was recorded as a function of time for 600 s. After OCP stabilization, impedance measurements were performed at respective corrosion potentials (E_{corr}) over a frequency range of 100 kH-0.1Hz, with a signal amplitude perturbation of 10mV. The potentiodynamic polarization tests were carried out in the potential range ±100 mV (with respect to OCP) at 0.001 mV/s scan rate. Nova 1.8 software was used for data fitting and calculation of the results obtained. The impedance and Tafel parameters were determined by curve fitting programme available in the above mentioned software. Each test was run in triplicate to verify the reproducibility of the data.

3. Results and discussion

Tartaric acid and dodecylbenzene sulphonic acid doped Poly(o-anisidine) nanoparticles were synthesized using in-situ emulsion polymerization technique. The epoxy-siloxane (ES) matrix was synthesized by the reaction between DGEBA and HPDMS by SN^2 mechanism and thus resulted in the formation of highly crosslinked ES network structure. Then, different wt. % of synthesised TA-DBSA-POA nanoparticles (0.5, 1 and 1.5 % by weight) was dispersed in 10.0 g of ES matrix through sonication followed by mechanical stirring. These nanoparticles and nanocomposites were characterized by different tecniques for the determination of

structure, size, morphology, composition, conductivity etc. The coatings of nanoparticles dispersed TA-DBSA-POA solutions were prepared and applied by brush technique on the finally polished and degreased surface of CS specimen of standard sizes. These nanocomposite coatings were further analysed for their anti-corrosive performance by various physico-mechanical, potentiodynamic polarization and electrochemical impedance spectroscopic techniques in varying concentration of NaCl (3.5 wt. %, 5 wt. % and 7 wt. %) media.

3.1 FT-IR Analysis

The FT-IR spectrum of pristine TA-DBSA-POA (Fig. 2) showed the presence of C=N (ν_{str}) and C=C (ν_{str}) stretching modes for the quinonoid (Q) and benzenoid (B) rings at 1595 cm^{-1} and 1505 cm^{-1} respectively. The peak at 1256 cm^{-1} showed C-O aromatic peak of benzene ring and the C–H bending vibration formed during protonation was confirmed by peak at 1112 cm^{-1} and C-O-C ether peak was observed at 1115 cm^{-1}. The band at 750 cm^{-1} revealed the presence of 1, 2 substitutions of NH_2 group at 1st position and OCH_3 group at 2nd position respectively. The peaks at 650 cm^{-1} is a characteristic peak of DBSA confirmed the doping with DBSA.

The FT-IR spectrum of ES (Fig. 2), showed a characteristic band at 3449 cm^{-1} associated with broad OH stretching of the hydroxyl groups, which confirmed the condensation reaction between epoxy and siloxane [27] corresponds to CH_2 asymmetric stretching (ν_{assym}) and the peak at 1670 cm^{-1} is attributed to the aromatic stretching vibration (ν_{ar}). The peaks appeared in the range of 1296 cm^{-1}-1184 cm^{-1} were correlated to the C–O–C of aryl alkyl ether, while the peak at 1095 cm^{-1} was attributed to the aryl alkyl ether symmetric stretching (sym). The oxirane ring peaks appeared at 910 cm^{-1}-830 cm^{-1} and Si-O vibration occurred at 660 cm^{-1} and 575 cm^{-1}

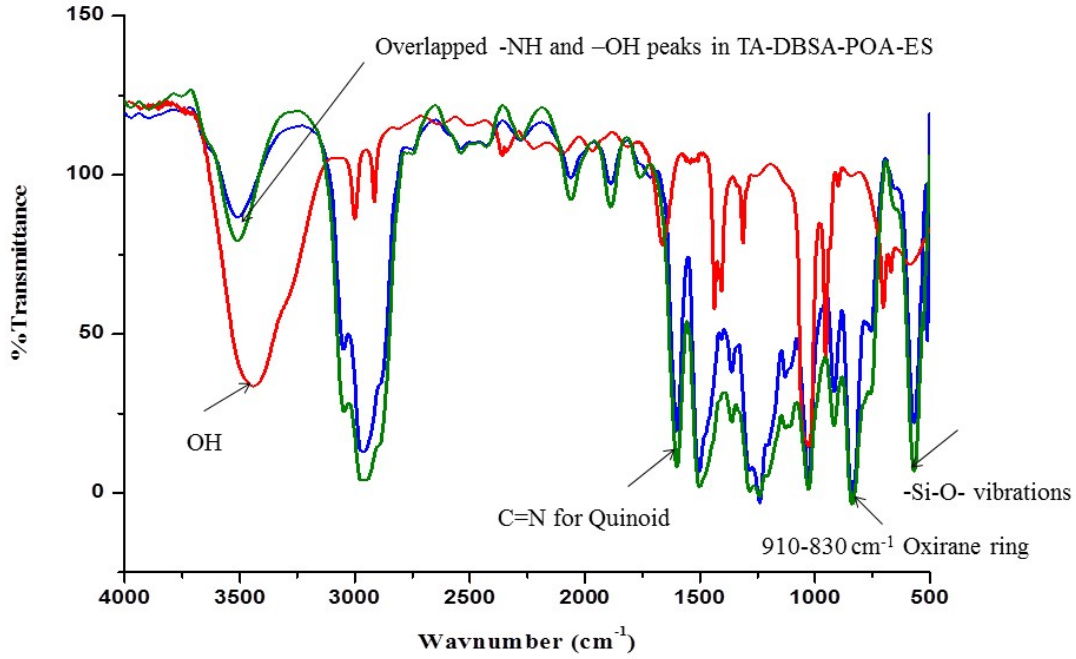

Fig. 2. FT-IR of (a) TA-DBSA-POA (b) ES matrix (c) 1.0 % TA-DBSA-POA-ES nanocomposite

The spectrum of 1.0% TA-DBSA-POA-ES (Fig. 2) showed OH stretching vibration peak at 3460 cm^{-1} with broader wavelength, which get shifted by 11 cm^{-1} as compared to ES matrix. The presence of peaks at 1390 cm^{-1}, 1438 cm^{-1} and 1508 cm^{-1} correspond to the bezenoid and quinonoid stretching modes of POA. The interaction between PANI chains and the DBSA was confirmed by the peak appeared at 1028 cm^{-1}. The benzenoid and quinoid vibration peaks were very intense and pronounced indicating the strong interaction between TA-DBSA-POA and ES, which was observed even at lower loading of TA-DBSA-POA filler. These bands suggested a conjugated pi-bond system, which may be attributed to the doped state of TA-DBSA-POA. As doping improves the conductivity levels forming polar on/bipolaron structures resulting in the increase of charge transfer in TA-DBSA-POA and higher electronic delocalization. The presence of conjugated double bands in the benzenoid and quinonoid rings permits electron mobility throughout the TA-DBSA-POA chains responsible for more electron delocalization, which resulted in the conducting nature of

nanocomposite. The NH stretching vibration band of TA-DBSA-POA overlaps the OH stretching vibration, which revealed an electrostatic interaction of NH group of TA-DBSA-POA and OH group of ES via strong hydrogen bonding (Fig. 3). All other characteristic peaks of ES, did not exhibit any major shift. Hence, the formation of TA-DBSA-POA-ES as nanocomposite was confirmed.

3.2 Mechanism of synthesis of ES and TA-DBSA-POA based TA-DBSA-POA-ES nanocomposite

In emulsion polymerization of conducting polymer, solubilisation locus, reactant monomers and their position in the micelles, significantly affects the reaction kinetics, selectivity, yield of the product and site for the incorporation of solubilizates in micelles. Kim et al., have explained that in case of non-polar, highly hydrophobic reactants .the solubilizates are located in the hydrocarbon core of the micelles[41]. It has been well accepted that the polar or surface active molecules are solubilized at the micelle–water interface. Ortho-anisidine exists in the form of anisidinium cation in acidic aqueous solution. Further Kim et al. have reported that in the synthesis of polyaniline nanoparticle, anilinium cations are adsorbed on the micellar surface by electrostatic interaction with anionic SDS molecules being fully exposed to the aqueous phase [41]. Similalry, anisidinium cations in o-anisidine monomer, these cations are adsorbed on the micellar surface by electrostatic interaction with anionic DBSA molecules being fully exposed to the aqueous phase as in case of PANI. However there are some portion of Na + as counter-ions would have interacted with the micelles, followed by the reduction of the charge density of micelles. Thus, referring to the literature, we assumed that most of the ortho-anisidine monomers were solubilized at the micelle-water interface. Obviously, some of them adsorb on the micellar surface and some in the aqueous phase. The solubilized o-anisidine or o-anisidinium molecules were oxidatively polymerized by APS present in the aqueous phase. Mainly, the reaction occurs at the micelle-water interface adjacent to the

surfactant head groups, as hydrated APS molecules could not penetrate into the micellar surface, as micelles [41] are not static and rigid entities . Probably they are in a dynamic equilibrium state with surfactant monomers in the solution and were dissociated into monomers, which were continuously associated into micelles. Thus all segments of the surfactant and solubilizates could be exposed to the water. As doping is the process by which polymers that are insulators are exposed to charge transfer agent. Here, in our work DBSA and TA were used as doping agent which provided electrons during the in process mechanism of formation of POA nanoparticles. TEM studies confirmed that presence of TA on the periphery of POA nanoparticles (Fig. 5c). Finally, o-anisidine molecules present in the aqueous phase would be incorporated readily into the micelles and grow into dimer, trimer or tetramer due to their increased hydrophobicity.

After the completion of reaction, synthesized TA-DBSA-POA nanoparticles are stabilized by adsorbed and incorporated DBSA molecules by electrostatic repulsive interactions. The mechanism of formation of TA-DBSA-POA-ES nanocomposite by solution blending method is purely based on the electrostatic interactions between nanoconducting polymer (filler) and matrix. The increase in viscosity with the increased loading of TA-DBSA-POA loading was due to the presence of Si-O-Si bonds between DGEBA backbones in heterogeneous manner that resisted the terminal epoxy group with the amine bond of TA-DBSA-POA, can be attributed to their ionic character. However, the presence of bulky methoxy pendant groups further prevented the curing reaction between NH groups of TA-DBSA-POA with OH group of ES

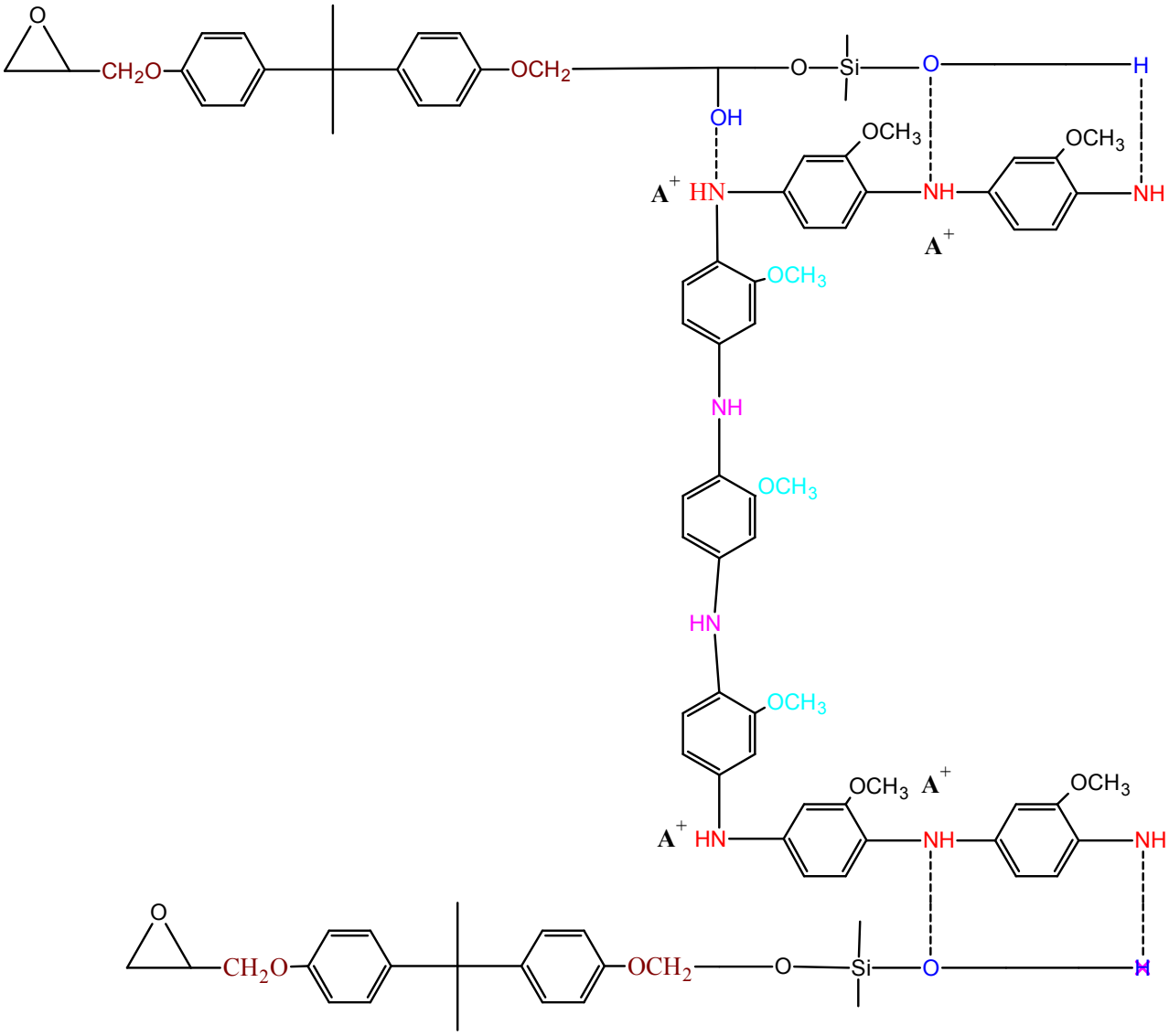

Fig. 3 Structure of TA-DBSA-POA-ES showing the interaction between TA-DBSA-POA and ES where A^- shows doping with TA and DBSA

matrix. Hence, TA-DBSA-POA acted as reinforcing part by forming network like structure through intermolecular hydrogen bonding between the OH group of ES and NH group of TA-DBSA-POA establishes the physical nature of interaction rather the chemical bonding (Fig. 3).

3.3 X-Ray Diffraction analysis

X-ray diffraction was used to explore the crystalline structure and phase identification of nanocomposites. The X-ray diffractogram of ES showed a diffraction peak spanning from 20-30^{o}. The presence of this broad hump indicated predominantly amorphous nature (Fig. 4). The size for virgin nanoparticle and that of nanocomposites were calculated using the Debye Scherer equation

$$D = 0.89\lambda / \beta \, Cos \, \theta$$

(Where D, λ and β represents size of crystallite, wavelength, full width half maximum respectively while θ represents diffraction angle). XRD diffractogram of TA-DBSA-POA showed pronounced peak at 20^{o} which can be correlated to (0 2 0) reflection [42]. The θ value evaluation using Scherer equation revealed TA-DBSA-POA nanoparticles with average particle size of 25-35 nm. The small angle XRD peak of TA-DBSA-POA-ES composite revealed the presence of microcrystalline domains and the diffraction pattern of composites with $2\theta = 25^{o}$. This peak exhibited shift of 5 ^{o} due to formation of composite structure having difference in structure and confirmation relative to TA-DBSA-POA nanoparticles. Thus confirming the semi-crystalline nature of composites which is further confirmed by TEM studies (Fig 4).

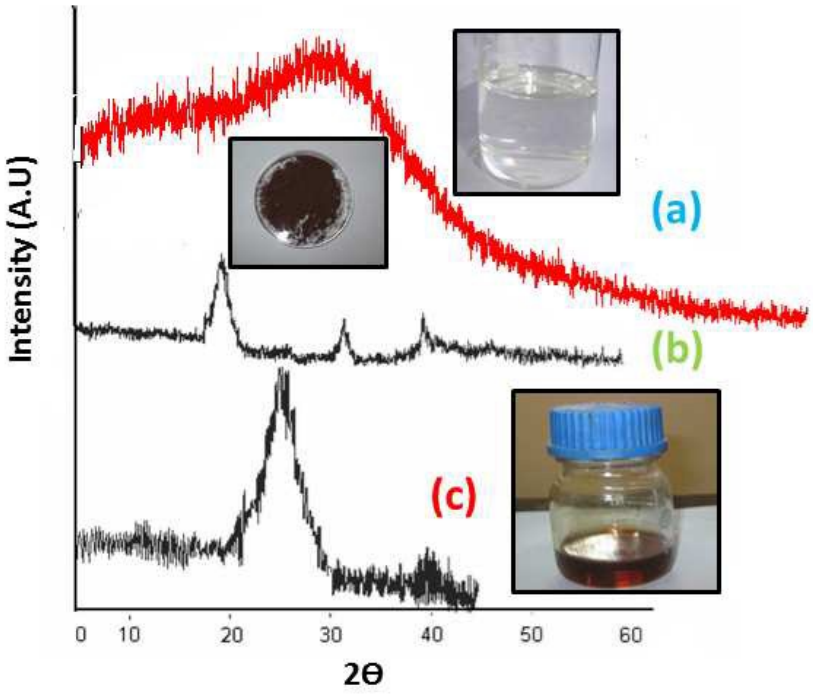

Fig. 4 XRD analysis of (a) ES matrix (b) TA-DBSA-POA (c) 1.0 % TA-DBSA-POA-ES nanocomposite.

3.4 Solubility Test:

The solubility behaviour of matrix, nanoparticles filler and their composites was investigated in various polar and non- polar solvents at room temperature. In case of nanocomposite (TA-DBSA-POA), the solubility was measured in terms of extent of their dispersibility and formation of the most miscible colloidal solution in polar and non-polar solvents. TA-DBSA-POA nanoparticles were well dispersed in polar solvents such as methyl alcohol, ethyl alcohol, DMSO, DMF and NMP while they fail to show their dispersion in non-polar solvents. TA-DBSA-POA contains oxygen atoms which is more electronegative and has lone pair of electrons, which induces electrostatic interaction between oxygen and hydrogen atoms of the constituent moieties [43]. Hence, the hydrogen atoms of organic solvents are attracted to the lone pair of electrons on the negatively polarized oxygen atom of TA-DBSA-POA,

forming hydrogen bond [5]. The lone pair electrons of oxygen atom are projected into the space away from the positively charged nuclei, promoting a considerable charge separation; therefore, dispersion was better in polar solvents than non-polar solvents. Similarly, for ES matrix and TA-DBSA-POA-ES nanocomposite, which have polar hydroxyls, oxirane, silicone and amino moieties, show more solubility in polar solvents than those of non-polar solvents (Table 1).

Table 1.

SOLUBILITY TEST:-

Solvent	**Solubility of**		
	ES	**TA-POA**	**TA-DBSA-POA-ES**
Xylene	Insoluble	Insoluble	**Insoluble**
DMF	Soluble	Soluble	**Soluble**
DMSO	Partly soluble	Soluble	**Soluble**
Toluene	Insoluble	Partially soluble	**Insoluble**
CCl_4	Insoluble	Insoluble	**Insoluble**
THF	Insoluble	Insoluble	**Insoluble**
Acetone	Partially soluble	Partially soluble	**Partially soluble**
Benzene	Insoluble	Insoluble	**Insoluble**
Ethylmethyl ketone	Soluble	Soluble	**Soluble**
Ethanol	Insoluble	Soluble	**Partially soluble**
Methanol	Soluble	Soluble	**Soluble**
NMP	**Insoluble**	**Soluble**	**Partially Soluble**

3.5 TEM and SEM of TA-DBSA-POA, ES and TA-DBSA-POA-ES

The TEM micrograph of ES revealed the formation of two phase matrix i.e. dark phase of silane (contrast) which was homogeneously dispersed in (Fig. 5a) grey phase of epoxy. The TEM micrographs of ES showed the compatibility of silane with the DGEBA matrix. The synthesis of fibular POA nanoparticles containing fine and small white particles of dia. ca. 25-35 nm was confirmed by TEM (Fig.5b) analysis. These non-agglomerated particles were modified by TA and DBSA dopants. The TEM micrograph (Fig.5c) illustrated the transformation of two phase morphology of doped POA nanoparticles from rod to spherical fibres. This can be attributed to the encapsulation of POA rod in TA and DBSA (Fig.5c-i-ii) . These doped nanoparticles are also acquiring intermingling long chain structure. Fig. 5d shows fine granular structure of ES containing well- dispersed nanoparticle of varying shape i.e. spherical to cubic fibres. This exhibits formation of homogeneous, compact, uniformly dispersed nanofillers composite coatings, which can be correlated to the improved properties of coating. SEM studies (Fig. 5e) were in concordant to TEM analysis. SEM micrograph of TA-DBSA-POA revealed the presence of nanofibres of doped POA.

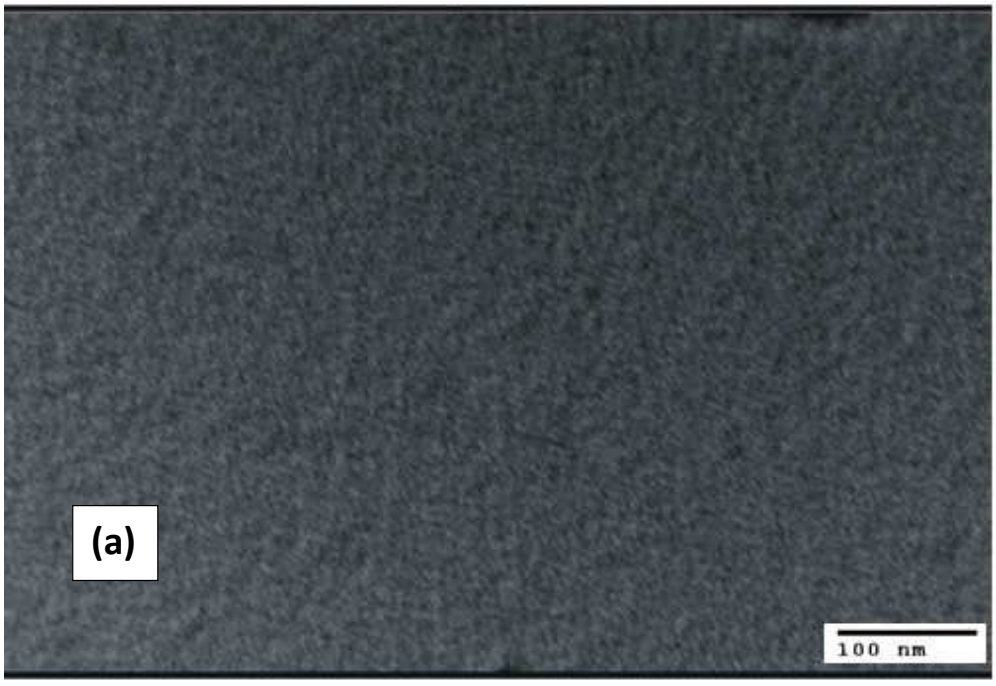

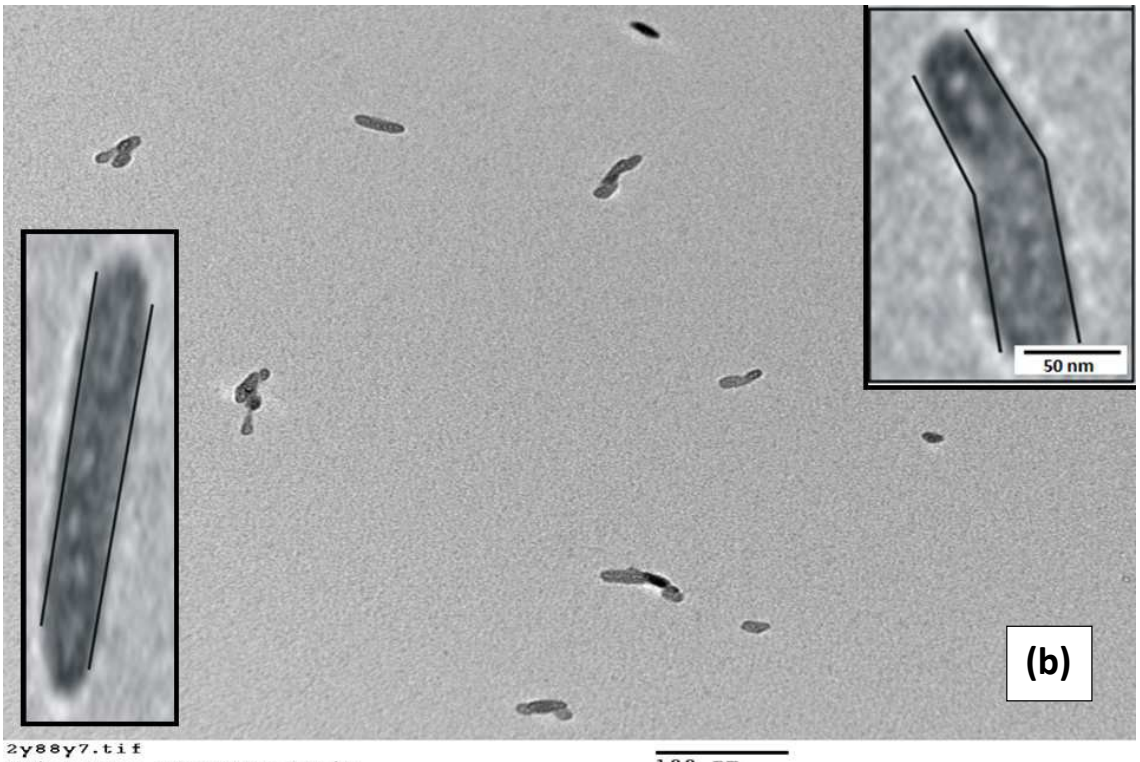

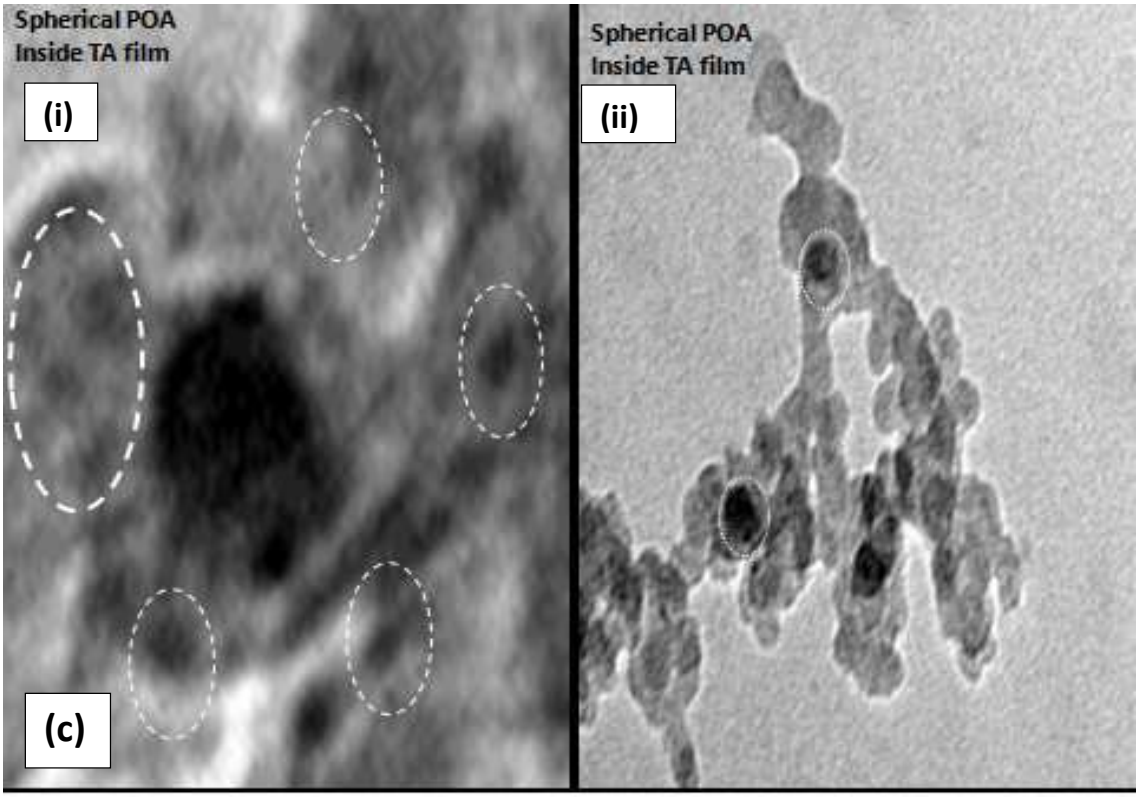

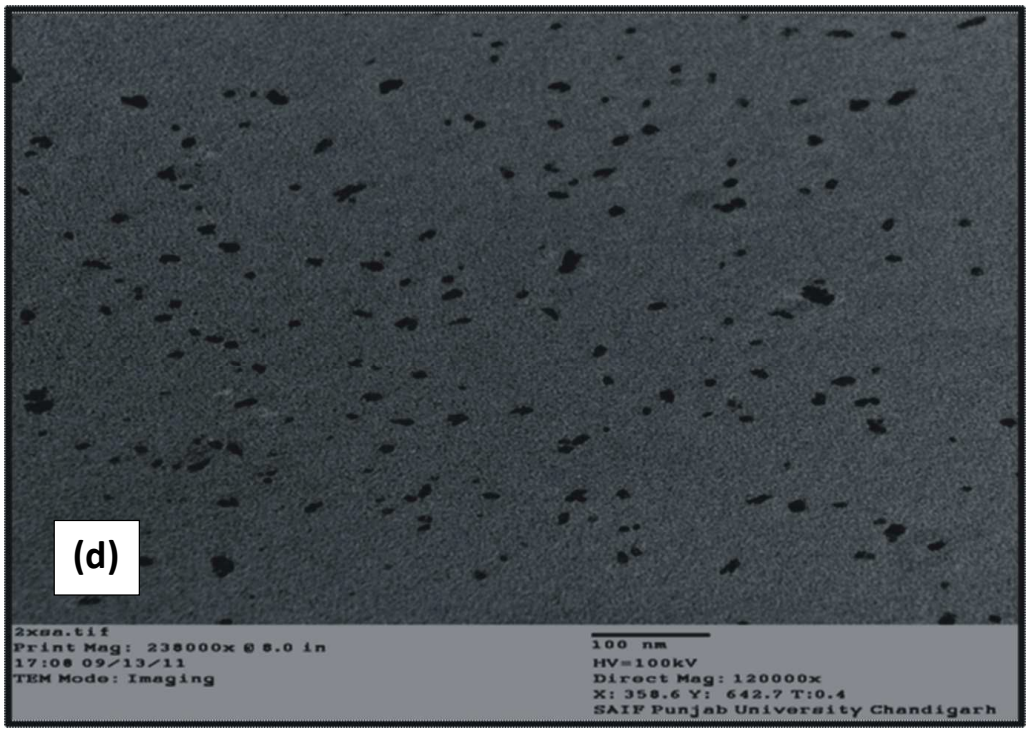

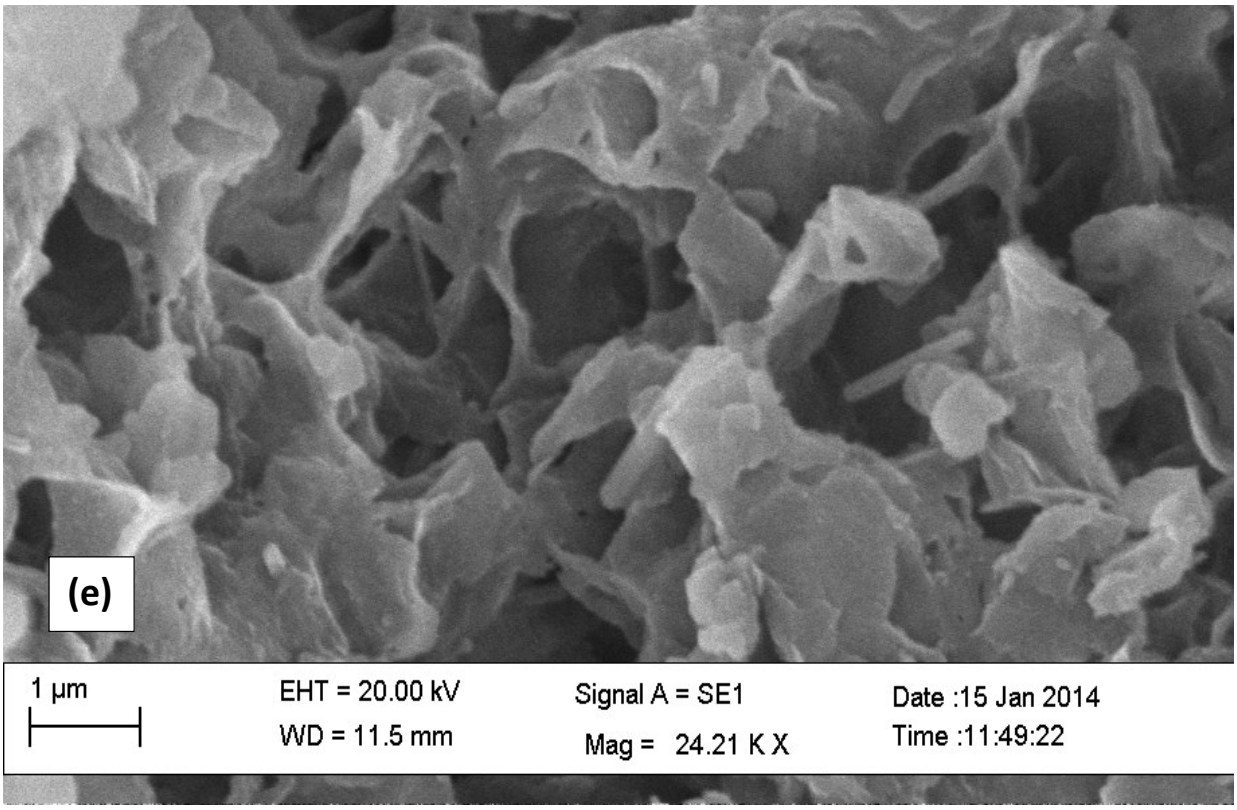

Fig. 5 TEM micrographs of **(a)** ES matrix **(b)** POA (inset enlarge view of POA nanofibres) **(c)** showing change in morphology (rod to spherical) of POA on doping with TA and DBSA **(d)** TEM micrographs of 1.0 % TA-DBSA-POA-ES

(e) SEM micrographs illustrating surface morphology of nanofibres of POA on doping with TA and DBSA

3.6 Thermal gravimetric analysis

Fig. 6 represents the TGA curves of ES and nCPs dispersed ES nanocomposite coatings. The thermal behaviour of TA doped POA (Fig. 6a) shows a three step weight loss process. The first weight loss (5-10 %) below 100 ° C is attributed to the loss of water and the second weight loss (20-50 %) ranging from 200 to 300 ° C is believed to be due to the elimination of acid dopant. The third weight loss starting at around 400 °C is assigned to the thermal decomposition of TA and DBSA doped POA backbone chains.

Further, the effect of incorporation of nanoparticles in ES matrix on the thermal stability of ES was investigated by TGA as shown in Fig. 6b-e. 5-10 wt.% weight loss occurred in the temperature range of 100 ◦C–170 ˚C due to the loss of absorbed solvent molecules. The first weight loss occurred at around 280 ˚C (Fig. 6b), due to the de-crosslinking of epoxy and siloxane. The second (350 ˚C- 450 ˚C) and third weight loss step (470 ˚C- 550 ˚C) could be assigned to the decomposition of the silica network. However, in case of nanocomposite coatings, degradation in material at higher temperature was observed in comparison to ES coatings. High thermal stability in nanocomposite coatings may be attributed to the uniform dispersion of TA-DBSA-POA-nanoparticles throughout the matrix and the strong interaction with the organic matrix. Besides, the presence of hydrogen bonding as evident from infrared spectroscopy was responsible for an increase in the thermal stability of the nanocomposites.

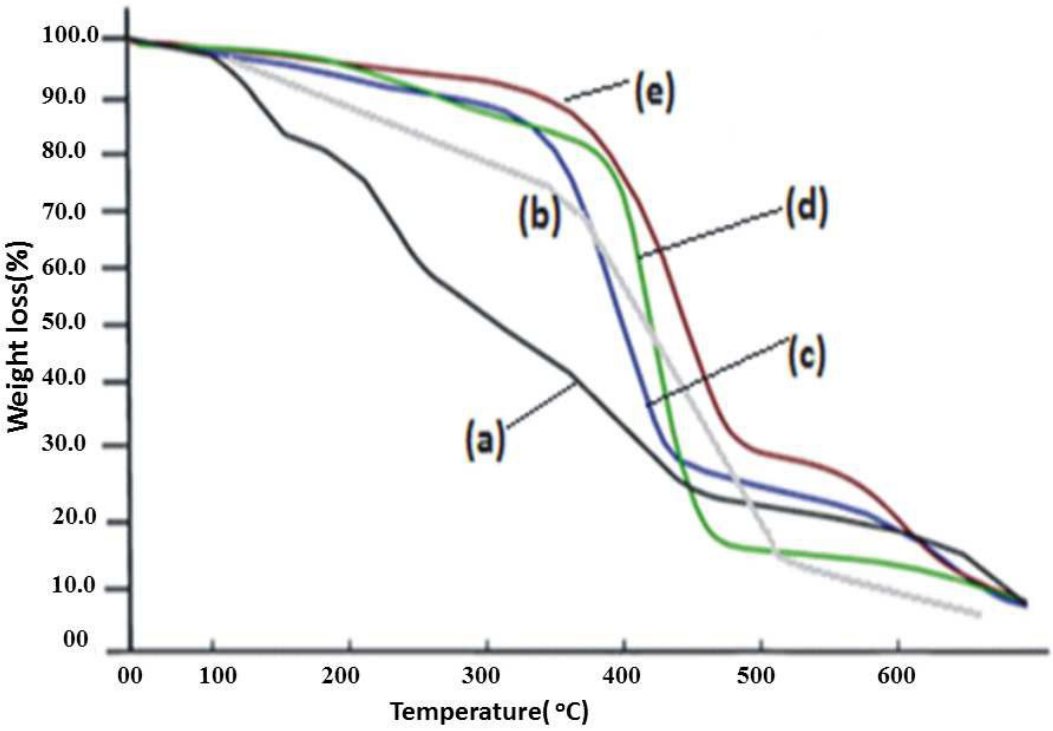

Fig.6. TGA of (a) TA-POA (b) ES (c) (b) 0.5 % TA-DBSA-POA-ES nanocomposite (d) 1.0 % TA- POA/ES nanoomposite (e) 1.5 % TA-DBSA-POA-ES nanocomposite

3.7 Physico-chemical and Physico-mechanical characteristisation

Fig.7 (a-d) provides the information about physico-chemical and physico-mechanical properties of ES matrix and TA-DBSA-POA-ES nanocomposites. The decrease in epoxy equivalent was observed with the loading of TA-DBSA-POA nanoparticle in ES matrix. The values of epoxy equivalent (EE) for ES, TA-DBSA-POA-ES, 1.0 TA-DBSA-POA-ES and 1.5 TA-DBSA-POA-ES were found to be 181, 179, 175 and 173 respectively, (Fig.7a). It indicated that the consumption of oxirane ring content increases with increase in TA-DBSA-POA interaction with ES matrix, which had increased with the increase in loading. The specific gravity of ES matrix and TA-DBSA-POA-ES nanocomposites increased with increase in loading. The value of specific gravity for ES, 0.5 % TA-DBSA-POA-ES, 1.0 %

TA-DBSA-POA-ES and 1.5 % TA-DBSA-POA-ES was 1.4, 1.6, 1.65 and 1.8 respectively. This also, supported the formation of a composites having higher density.

The gloss value had an inverse relationship with loading of TA-DBSA-POA. The gloss values for 0.5 % TA-DBSA-POA-ES, 1.0 %TA-DBSA-POA-ES and 1.5 % TA-DBSA-POA-ES were 42 ^{o}, 39 ^{o} and 36 ^{o} respectively. This can be attributed to the increase in the TA-DBSA-POA loading in ES lead to the formation of dense structure and opaque nature of TA-DBSA-POA (Fig.7b) The dry-to-touch and dry-to-hard times of TA-DBSA-POA-ES composites exhibited a large decrease (Fig. 7c).

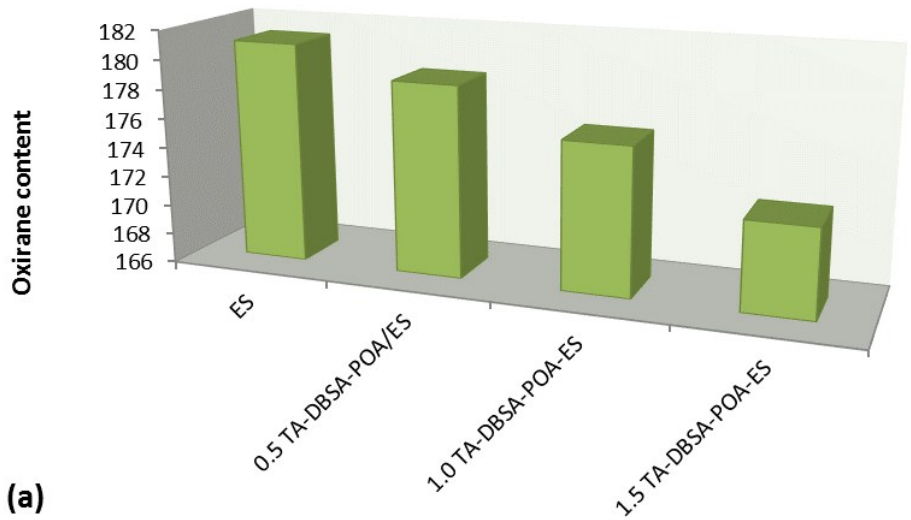

(a)

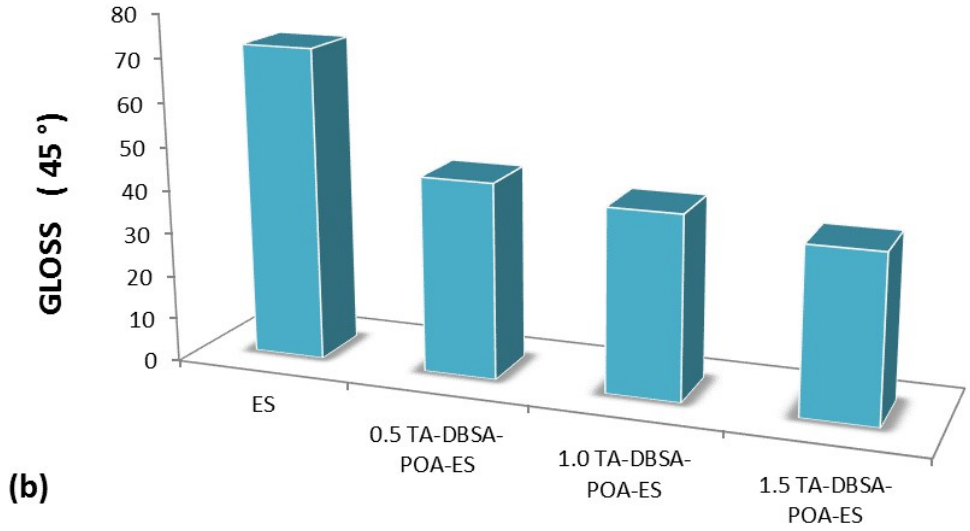

(b)

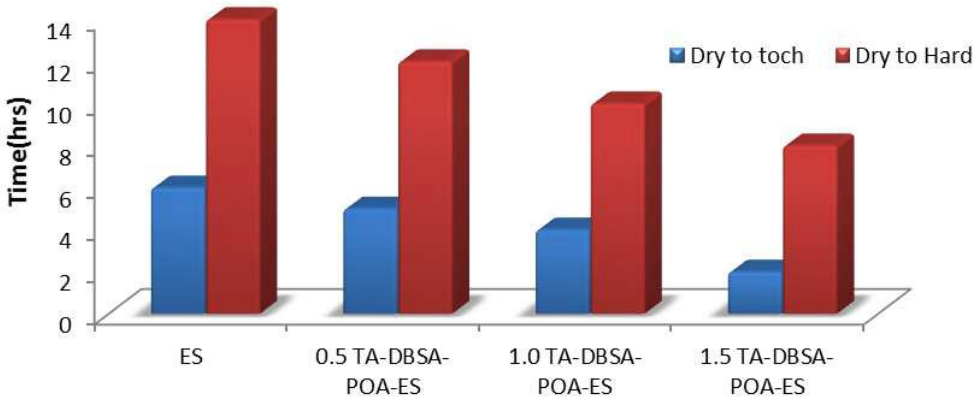

(c)

The dry-to-touch time for pristine ES was 6 h while the dry to-hard time was 14 h. The inclusion of DBSA-TA- POA resulted in a gradual decrease in the dry-to-touch time and dry to-hard times, which was found to be 5 h and 12 h for 0.5% TA-DBSA-POA-ES, 4 h and 10 h for 1.0% TA-DBSA-POA-ES), 2 h and 8 h for 1.5% TA-DBSA-POA-ES, respectively, the trend can be attributed, to the extent of crosslinking occurred in the cured

structure of the TA-DBSA-POA-ES . It was found that the scratch hardness values increased from 4 to 12 kg as the loading of TA-DBSA-POA in ES increased from 0.5 to 1.5 wt%. The increase in scratch hardness values assigned for an intimate mixing of two components and the increase in adhesion at the interface of TA-DBSA-POA-ES nanocomposite coating and the surface of the substrate. The presence of strong hydrogen bonding between ES matrix and TA-DBSA-POA was also responsible for the increase in adhesion. The nanocomposite coatings with different loadings of TA-DBSA-POA passed 1/8 inch bend (flexibility) test and the impact resistance test (150 lb/inch). The coatings were found to be flexible as they bend without any damage or fracture. The higher scratch hardness, flexibility and impact resistance can be correlated to the polar hydroxyls, oxirane and siloxane moieties present in the backbone of the polymeric chain of nanocomposites and also to the presence of strong hydrogen bonding. The MEK double rub cycle test values of all the coated CS were higher than 400 cycles.

3.8 Conductivity Studies

Conductivity measurements were carried out at ambient conditions. The conductivity value of pristine POA was found to be 5.02 E-3 S/cm and that of TA-DBSA-POA (Fig. 7d) was 2.09 S/cm. Upon loading of 0.5 wt. % of TA-DBSA-POA in ES, the conductivity decreases in regard of insulating nature of matrix. On increased loading, a slight increase in conductivity occurred (0.5 to 1.5 wt. %).

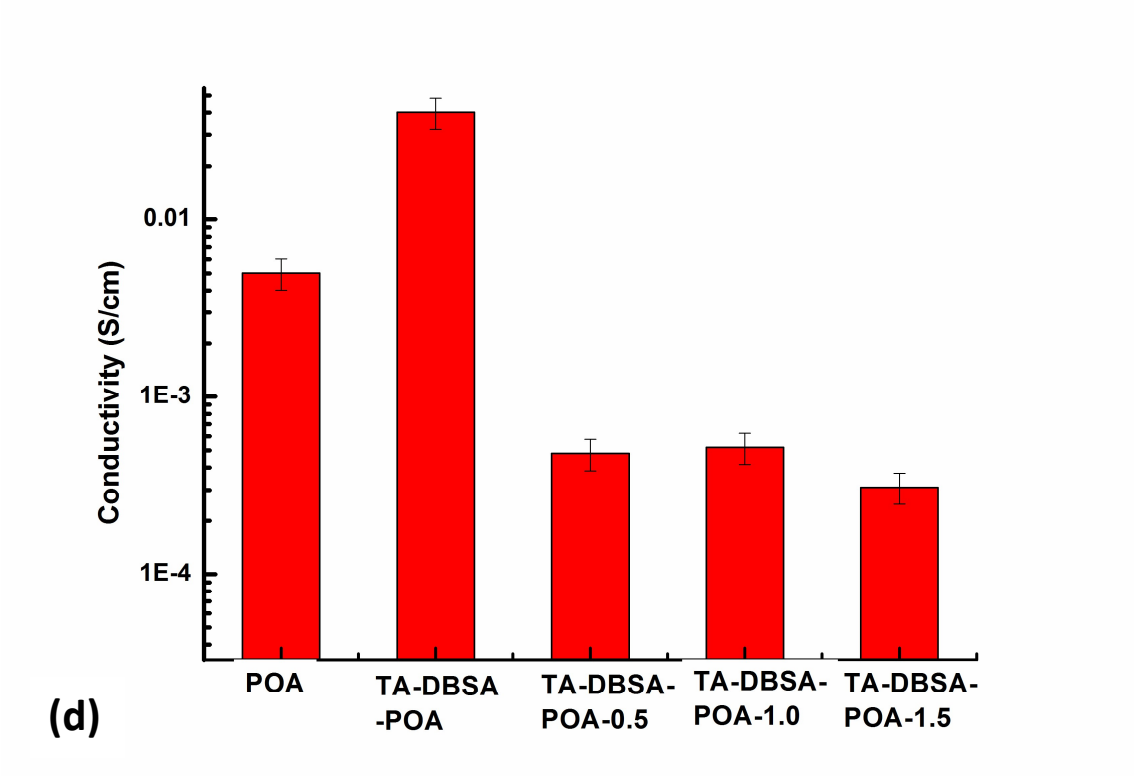

Fig.7 Graphs showing variation of **(a)** oxirane content with loading **(b)** gloss with loading **(c)** DTT and DTH with loading **(d)** conductivity

The conductivity values for TA-DBSA-POA-ES-0.5, TA-DBSA-POA-ES-1.0 and TA-DBSA-POA-ES-1.5 were found 4.8 E-4 S/cm, 5.2 E-4 S/cm and 3.1 E-4 S/cm respectively. The threshold value for conductivity was found in case of TA-DBSA-POA-ES-1.0 nanocomposite.

3.9 Salt spray test

Salt Spray test (SST) was conducted for a period of 15 days in NaCl solution. The uncoated CS specimen was tested as a control. Initially, the coated and uncoated specimen shows a glossy and shiny surface, with the exception of a greenish colour on TA-DBSA-POA-ES coated specimen. After, 48 h of SST the uncoated specimens lost its glossy shiny appearance and the entire surface covered with dark grey areas, exhibiting pitting and gazing at the surface along with the significant corrosion damage while, the ES coated specimens show

loss in gloss after 144 h, while that of TA-DBSA-POA-ES nanocomposite coated samples lost their gloss only after 288 h and no degradation was observed even after 320 h for TA-DBSA-POA-ES coating while for ES coated CS show some deterioration after this period. This clearly shows that TA-DBSA-POA-ES nanocomposite protects the CS from corrosion in saline medium.

3.10 SEM-EDAX

After 360 h of SST, the SEM images showed the deposition of salt (NaCl), on the surface however, no cleavage of the matrix was visually observed. The EDAX measurement of the coated surface exhibited no metallic iron, only the presence of slight deposition of chloride ions was observed. The improved corrosion protection performance of nanocomposite coatings was synergistically correlated to the generation of hydrophobic surface, barrier and redox protection due to dispersed POA nanoparticles (optical micrograph Fig. 8a-b) and after

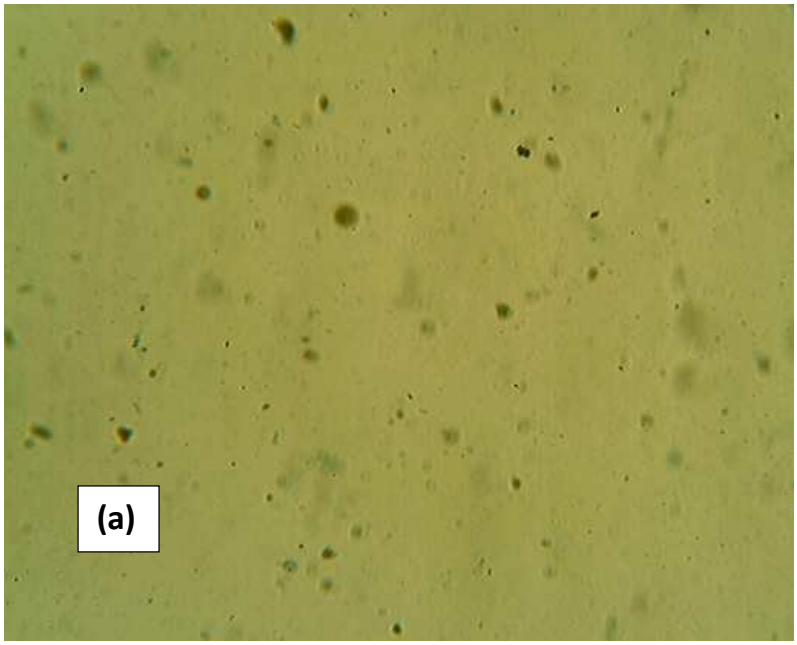

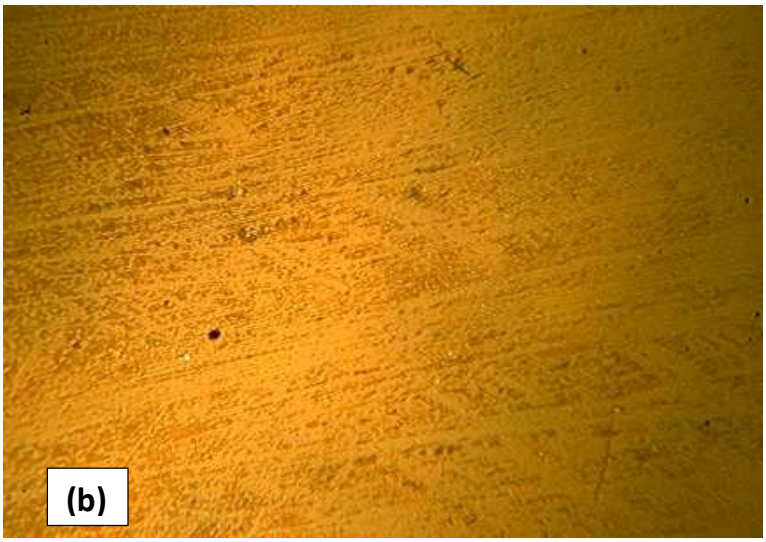

Fig.8(a) Optical micrograph of TA-DBSA-POA-ES coated CS

(b) TA-DBSA-POA-ES coated CS after SST

salt spray test.

They are responsible for increased crosslink density and formation of compact coating surface, which did not allow the penetration of corrosive ions to the coating-metal interface (Fig. 9),

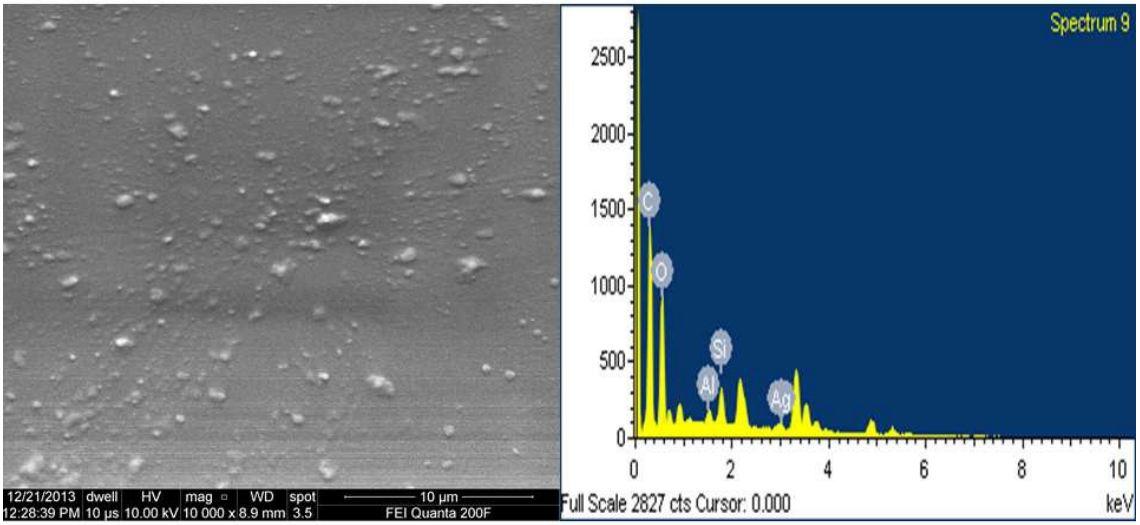

Fig.9 SEM micrograph of TA-DBSA-POA-ES coated CS and EDAX spectra.

thus the improved corrosion resistance performance of the TA- DBSA- POA-ES coating as compared to that of plain ES coatings (Fig. 10).

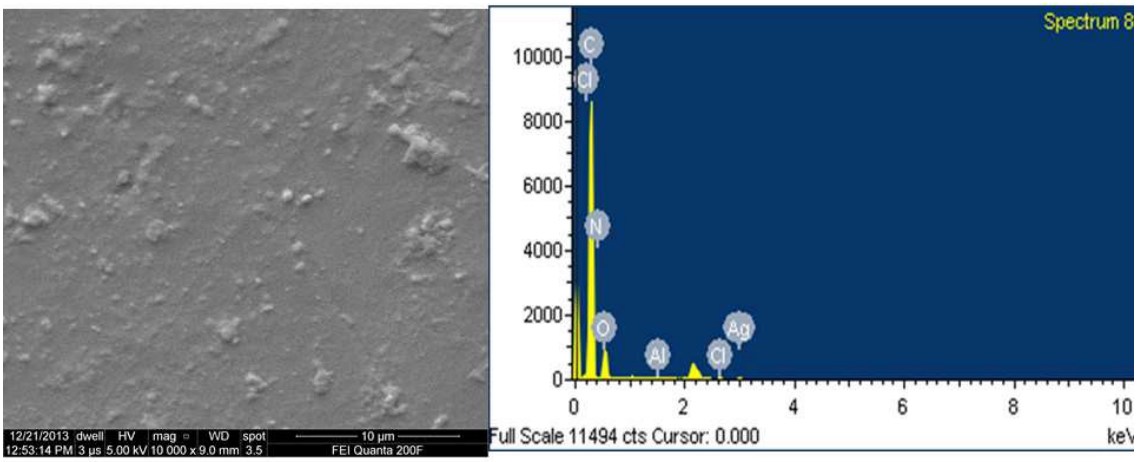

Fig.10 SEM micrograph of TA-DBSA-POA-ES coated CS and EDAX spectra after SST

3.11 Potentiodynamic polarization studies

The polarization measurements are used to monitor the electrochemical corrosion rate and mechanism of anodic and cathodic partial reactions as well as indentifying the effect of an additive on either partial reaction. The potentiodynamic polarization curves and corresponding electrochemical parameters were recorded for ES coated and TA-DBSA-POA-ES composite coatings on CS in different corrosive ion concentration (3.5, 5.0 and 7.0 wt.% NaCl solution) are shown in Fig. 11 and Table 2(a-c) respectively. Corrosion potential and corrosion current density were obtained by extrapolation method in which intersection of anodic and cathodic curves were extrapolated at the point of intersection. The well-known Stern-Geary equation was used to calculate the polarization resistance R_p.

$$R_p = \frac{b_a b_c}{2.303 (b_a + b_c) I_{corr}}$$

In 3.5 % NaCl, CS samples coated with ES exhibited the lowest corrosion potential (-0.2775V) and the highest corrosion current density (6.7084E-6 A/cm^2). In contrast, for the

composite coatings containing TA-DBSA-POA-ES, the corrosion potential significantly increased and the corrosion current decreased, which indicated that the TA-DBSA-POA-ES composite coatings on CS samples provide higher corrosion resistance. Moreover, increasing the content of TA-DBSA-POA caused a gradual increase in the corrosion potential and simultaneously showed the decrease in the corrosion current, therefore the corrosion resistance was improved.

The superior corrosion protection of TA-DBSA-POA-ES coatings to CS may be correlated to the fact that the nanofiller were homogeneously dispersed in matrix. The polar pendant functional groups of filler and ES induced adhesion at coating-CS interface. These polar groups developed strong electrostatic interaction between labile positive charges present on the metal surface, which induced strong adhesion at coating metal interface. The other reason being the hydrogen bonding present between ES and TA-DBSA-POA-ES as shown in Fig 3, which also reduced the effective area of corrosion through the blockening of reaction sites

Similarly, in 5.0 wt. % NaCl solution, the E_{corr} and $_{Icorr}$ values follows the same trend for different compositions of TA-DBSA-POA-ES coatings as discussed in the above section. However, a large negative shift towards active side was observed for 1.5 wt.% TA-DBSA-POA-ES coatings as compared to 1.0 wt.% and 0.5 wt.% DBSA-POA-ES coatings, as we increased the concentration of NaCl from 5wt.% to 7wt%. Nevertheless, the 1.5 wt.% TA-DBSA-POA-ES coatings still protect the underlying metal substrate from corrosive ions in relative to plain ES coatings. The low corrosion protective performance of 1.5 wt. % TA-DBSA-POA-ES coatings at higher concentration of NaCl i.e. 7 wt. % may be attributed to the destruction of Fe_2O_3 layer formed [44].

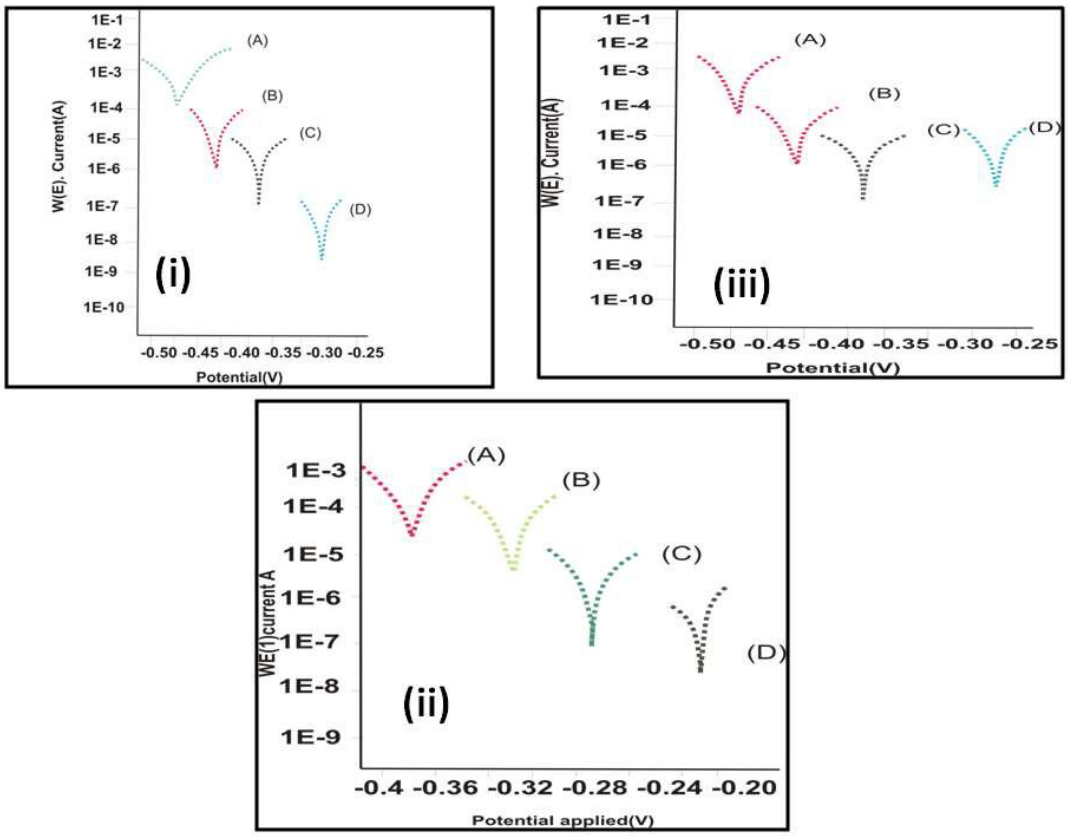

Fig. 11 PDP curves of TA-DBSA-POA-ES in (i) 3.5 wt% NaCl (ii) 5.0 wt% NaCl (iii) 7.0 wt% NaCl medium where ((A) ES (B) 0.5-TA-DBSA-POA-ES (C) 1.0-TA-DBSA-POA-ES (D) 1.5-TA-DBSA-POA-ES

3.12 Electrochemical impedance spectroscopy;

EIS experiments were conducted in order to understand the kinetics of the electrochemical corrosion processes and the role of nanocomposite coatings on CS and how they were modified by the incorporation of nanoparticles in ES**.** To further study anti-corrosive performance of composite coatings, the EIS was adopted. Fig. 12 (a-d) depicts Nyquist plots of TA-DBSA-POA-ES coatings in various concentration of NaCl (3.5 %, 5.0% and 7.0% respectively). The Nyquist plots showed the formation of single semi-circle having one time constant having three components R_s as solution resistance, Rpore as pore resistance and Cc

as coating capacitance. (Fig.12). All Nyquist plots were close to a semicircle, and the diameter of which was equal to the charge transfer resistance (R_{ct}) for CS samples.

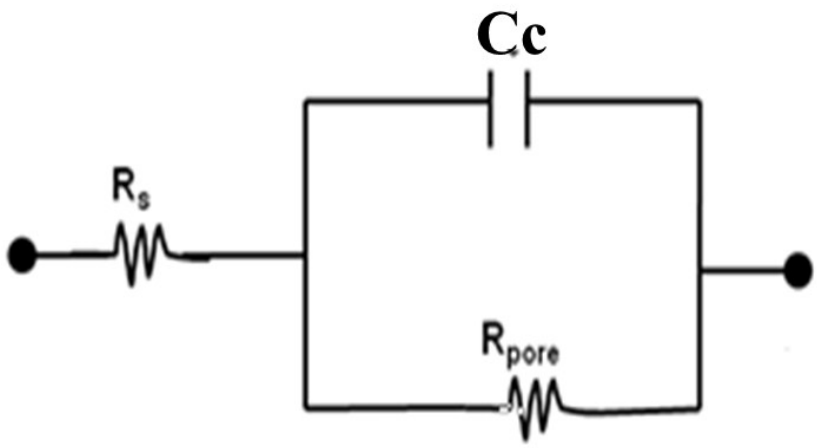

Fig.12 Equivalent circuit model

In case of 3.5 % NaCl medium **Fig. 13(i)**, R_{pore} value increased and C_c value decreased for TA-DBSA-POA-ES coated CS as compared to plain ES coatings This clearly indicated that the introduction of TA-DBSA-POA in ES matrix enhanced the anti-corrosive performance of epoxy-PA coatings. Besides, as the loading of TA-DBSA-POA-ES was introduced in ES matrix, corrosion protective performance was increased in the said medium. The results demonstrated that the coatings containing CPs passivate the CS substrate and thus shift the potential toward noble direction in comparison to the plain ES. Further, literature reveals that once the CP s like PANI[14], PPy[4], and their derivatives [45] are introduced, coating resistance could be maintained relatively higher values, indicating the better protection performance of CP containing coatings than that of pure epoxy coatings.[46] Besides, it was found that the value of R_{ct} gradually became bigger with increasing the TA-DBSA-POA content. The R_{ct} approached the maximum at 1.5 wt. %, followed by 1.0 wt. % TA-DBSA-POA-ES, 0.5 % TA-DBSA-POA-ES and plain ES coatings.

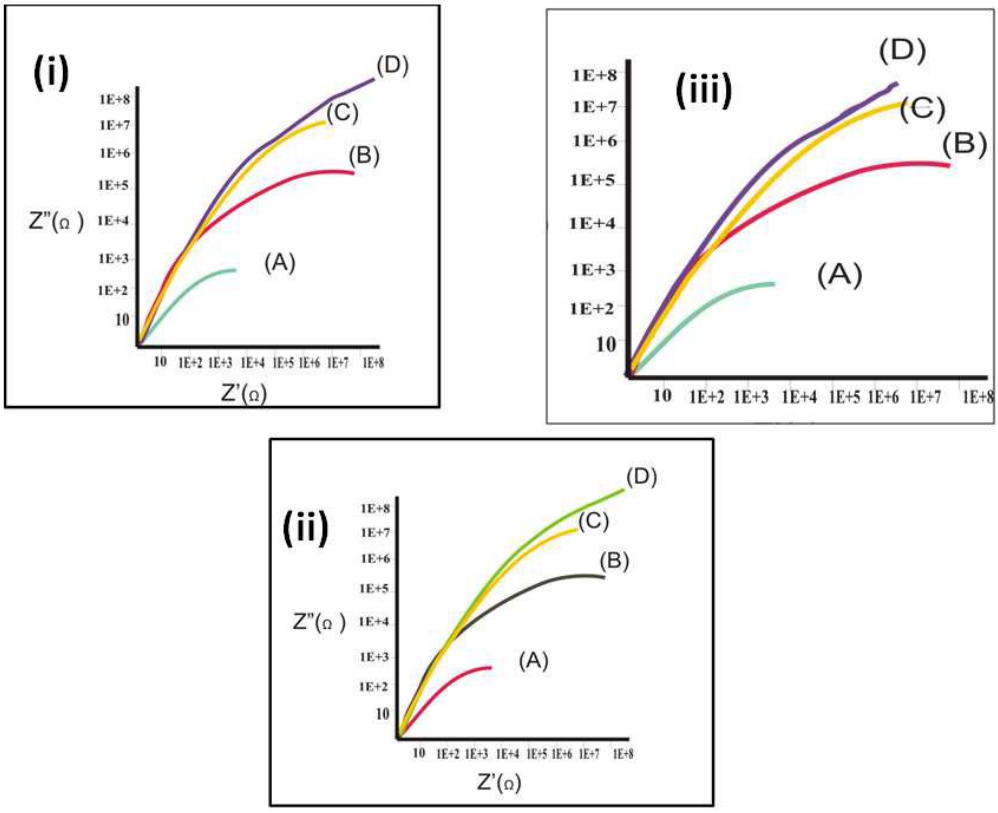

Fig. 13 EIS spectra of TA-DBSA-POA-ES in (i) 3.5 wt% NaCl (ii) 5.0 wt% NaCl (iii) 7.0 wt% NaCl medium where ((A) ES (B) 0.5-TA-DBSA-POA-ES (C) 1.0-TA-DBSA-POA-ES (D) 1.5-TA-DBSA-POA-ES

In case of 5.0 % NaCl medium **Fig. 13(ii)**, R_{pore} and C_c values followed the same trend for TA-DBSA-POA-ES and ES coated nanocomposite coatings as explained above. The behaviour of all the ratios remarkably followed the same trend as above in case of 3.5% NaCl. However, a declination in R_{pore} and C_c values for 1.5 wt. % TA-DBSA-POA-ES relative to other compositions was observed as we increased the concentration of NaCl from 5 wt.% to 7 wt. % **Fig. 13(iii)**. Although, the higher concentration of NaCl protects the CS substrate by forming passive layer in comparison to plain ES coatings, however, the corrosion process is not fully

Table 2(a). Electrochemical parameters obtained from PDP and EIS studies for uncoated and coated CS in 3.5 % NaCl at room temperature.

Sample Code	Ecorr (V)	Icorr (A cm^{-2})	Rp (Ω)	Rpore Ω)	Cc(farad)
CS	-0.33285	0.0005519 7	33.469	$2.4x10^{3}$	$7.1x10^{-5}$
Epoxy-siloxane (ES)	-0.28424	0.0002659 4	967.07	$6.1x10^{3}$	$2.9x10^{-7}$
0.5-TA-DBSA-PoA-ES	-0.28899	0.0000021 884	3228.3	$2.3x10^{5}$	$3.6x10^{-9}$
1.0-TA-DBSA-PoA-ES	-0.22403	0.0000013 6	1799.1	$3.1x10^{7}$	$7.8x10^{-10}$
1.5-TA-DBSA-PoA-ES	-0.20508	0.0000024 8	2226.7	$5.2x10^{7}$	$9.8x10^{-10}$

Table 2(b). Electrochemical parameters obtained from PDP and EIS studies for uncoated and coated CS in 5% NaCl at room temperature.

Sample	Ecorr (V)	Icorr (a cm^{-2})	Rp (Ω)	Rpore (Ω)	Cc(farad)
CS	-0.24017	7.9416E-4	7032.2	$1.2x10^{3}$	$1.8x10^{-3}$
Epoxy-siloxane(ES)	-0.26254	5.9084E-6	39272	$2.2x10^{4}$	$2.32x10^{-4}$
0.5-TA-DBSA-PoA-ES	-0.38021	2.4207E-7	29121	$1.27x10^{6}$	$9.67x10^{-6}$
1.0-TA-DBSA-PoA-ES	-0.40885	4.3782 E-8	7751.1	$1.72x10^{7}$	$7.9x10^{-10}$
1.5-TA-DBSA-PoA-ES	-0.50023	5.226 E-8	8872.5	$2.12x10^{7}$	$8.19x10^{-10}$

Table 2(c). Electrochemical parameters obtained from PDP and EIS studies for uncoated and coated CS in 7% NaCl at room temperature.

Sample	Ecorr (V)	Icorr (a cm^{-2})	Rp (Ω)	Rpore (Ω)	Cc(farad)
CS	-0.2217	9.9416E-4	7012.2	$1.2x10^{3}$	$1.8x10^{-3}$
Epoxy-siloxane (ES)	-0.22254	6.9084E-6	49272	$2.2x10^{4}$	$2.32x10^{-4}$
0.5-TA-DBSA-PoA-ES	-0.34031	3.4207E-7	29721	$1.27x10^{6}$	$9.67x10^{-6}$
1.0-TA-DBSA-PoA-ES	-0.380885	4.3782E-8	8751.1	$1.72x10^{7}$	$7.9x10^{-10}$
1.5-TA-DBSA-PoA-ES	-0.340985	2.3882E-8	28771	$2.31x10^{5}$	$1.27x10^{-6}$

protected. This result may be attributed to the presence of higher concentration of chloride ions which destroy the passive layer. Further, literature also showed that the present conducting polymer based system exhibits far excellent corrosion resistance potential as compared to other reported systems.

3.13 Raman spectroscopy:

The presence of the passive layer was determined by Raman spectra. As shown in Fig. 13, the bands on the surface of TA-DBSA-POA-ES coated CS immerged for 15 days in 5 wt % NaCl aqueous solution were stronger in comparison to ES coated CS. The presence of 526 cm^{-1} was assigned to chlorination of TA-DBSA-POA-ES, the absence of such modification in ES without conducting polymer filler may be an indication that the structural changes observed

in ES as were induced by filler and they improved the corrosion protection performance.

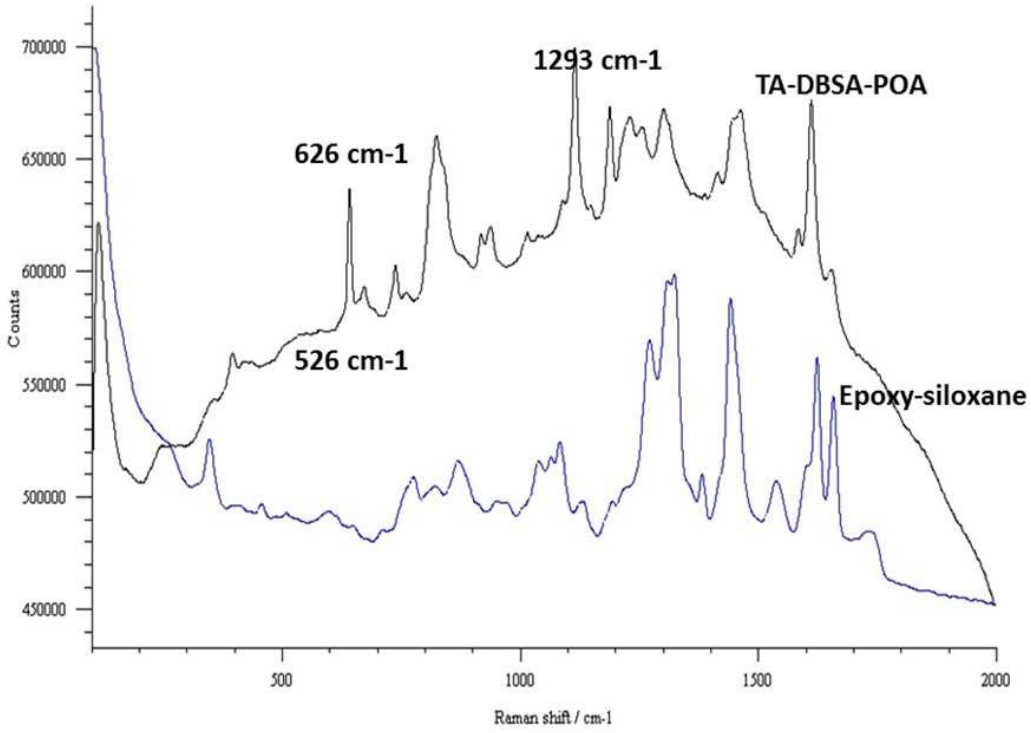

Fig.13 Raman spectra of ES and TA-DBSA-POA-ES coated CS after SST to confirm ferric oxide layer formed.

The bands at about 216, 281 cm $^{-1}$, and 1293 cm $^{-1}$ were assigned to α-Fe_2O_3 [Fig. 13]. This indicates that the surfaces of CS coated by TA-DBSA-POA-ES formed passive layers, which are composed of α-Fe_2O_3 [23]. Further Raman spectroscopy depicted some kind of interaction between ES matrix and TA-DBSA-POA filler.

3.14 Mechanism of corrosion protection

Corrosion occurs in the presence of water, salts and oxygen; during which iron or steel undergo an electrochemical process in which different locations of the iron surface act as electrodes. At the local anode, iron is oxidised to soluble Fe^{2+} and Fe^{3+} ions:

$$n\mathrm{Fe(s)} \longrightarrow m\mathrm{Fe}^{2+}(\mathrm{aq}) + (n-m)\mathrm{Fe}^{3+}(\mathrm{aq}) + 3(n-m)\mathrm{e}^{-} \qquad (1)$$

At the local cathode, hydroxide ions are formed:

$$O_2(aq) + 2H_2O(l) + 4e^- \longrightarrow 4OH^-(aq) \qquad (2)$$

Rust, which for CS subsequently, is composed of FeO, Fe_2O_3, Fe_3O_4 and other mixed oxides, Fe $(OH)_x$, and Fe^{x+} salts (chlorides, sulfates *etc*). This highly irreproducible and irregular composition opens up new surfaces for self-catalytic growth - mainly Fe^{3+} salts acting as rust formation catalysts. Rust that forms this way does not adhere well on the iron surface. The mechanism of the corrosion protection of CS provided by the conducting polymers is well reported in the literature [22].It was considered that the conducting moieties of conducting polymers acted as an active coating in the reaction taking place across the polymer coated and metal-electrolyte interface. In the presence of the conducting polymer (TA-DBSA-POA) coating, a completely different galvanic process occurs, in which TA-DBSA-POA replaces iron as the cathode due to its metallic property, as it is situated like PANI slightly less noble than silver in the galvanic series. This arrangement is relatively evenly distributed over the whole surface. It involves Fe-oxidation by TA-DBSA-POA-ES (the more noble metal, Emeraldine salt ES), which is thereby reduced to Leucoemeraldine base (LE); further oxidation of Fe (II) to Fe (III) and reoxidation of LE to TA-DBSA-POA(ES) via the Emeraldine base EB occur both by oxygen; and Fe_2O_3 deposition by resulting OH^-. This scheme shows furthermore, that TA-DBSA-POA coating is different from conventional coatings in that it does not protect simply by offering a physical barrier but it acts as a redox catalyst, and the full catalytic cycle (ES to LE to EB and back to ES) protect the metal surface as long as the mechanical integrity of the polymer film remains intact. By TA-DBSA-POA coating, a remarkable corrosion potential shift ('ennobling') and an iron oxide layer formation ('passivation') together lead to a significant anticorrosion effect. On the above, the excellent adhesion of TA-DBSA-POA-ES nanocomposite coatings, with the metal substrate due to the uniform dispersion of POA nanoparticles in a matrix as evident from SEM-EDAX

study (Fig.13), which can be corroborated for the superior anti-corrosive performance. Based on these observations, the suitable mechanism has been visualized and presented in graphical abstract.

3.15 Chemical resistance

The results of chemical resistance of all the ratios of TA-DBSA-POA-ES and ES in different chemical environments are given in the Table 3.

Table 3. Chemical resistance of the ES and TA-DBSA-POA-ES in different chemical environment after 15 days.

Chemical environments	ES	0.5%	1.0 %	1.5%
Aq HCl (5%)	c	b	b	a
Aq NaOH(5%)	c	b	b	b
Aq NaCl(5%)	b	c	a	a

(a) The film remains intact and unaffected slight loss in gloss observed after 15 days.

(b) The film remains intact and unaffected slight loss in gloss observed after 12 days.

(c) The film remains intact and unaffected slight loss in gloss observed after 10 days.

The coatings showed excellent aqueous alcohol resistance as well as very good aqueous alkali and acid resistance due to the presence of high hydrogen bonding between TA-DBSA-POA and ES as well as strong chemical linkages. With increase in the loading of TA-DBSA-POA-ES from 0.5 wt % to 1.5 wt%, the alkali and acid resistance increased, though decrements are marginal.

4. Conclusion:

Tartaric acid–dodecylbenzenesulphonic acid doped Poly(o-ansisidine) nanofibres were successfully synthesized via emulsion polymerization in-situ and their nanocomposites were prepared using epoxy-siloxane matrix by solution blending method. These composites were characterized by FTIR, XRD, UV-visible and TEM. The thermal stability of nanocomposites increase with the increase in loading of nanoparticles. The conductivity of nanoparticle and that of nanocomposite was found remarkably in the order of 10^{-3} S/cm and 10^{-4} S/cm respectively. The nanocomposite coatings exhibited promisily enhanced physico-mechanical properties in comparison to virgin epoxy-siloxane coatings owing to the uniform dispersion of nanofibres in matrix and intermolecular hydrogen bonding. Raman spectra confirmed the formation of Ferric oxide layer. The PDP and EIS studies revealed that with the increased loading of nanoparticles, the corrosion resistance performance remarkably increased upto 3.5 wt. % however, at 7 wt. % NaCl the increase in corrosion resistance property observed only upto 1.0 wt. % of nanocomposite coating, as a slight decrease in corrosion resistant property was found in case of 1.5 wt. % loading.

References:

1. R. Akid, M. Gobara and H. Wang, *Electrochim. Acta.*, 2011, **56**, 2483-2492.
2. R. Arefinia, A. Shojaei, H. Shariatpanahi and J. Neshati, *Prog. Org.Coat.*, 2012, **75**, 502-508.
3. D. R. Baer, P. E. Burrows and A. A. El-Azab, *Prog. Org.Coat*., 2003, **47**, 342-356.
4. İ. Çakmakcı, B. Duran and G. Bereket, *Prog. Org.Coat*., 2013, **76**, 70-77.
5. G. M. Abou-Elenien, A. A. El-Maghraby and G. M. El-Abdallah, *Synthetic Met.*, 2004, **146**, 109-119.
6. A. G. MacDiarmid, *Synthetic Met.*, 2001, **125**, 11-22.
7. M. L. Zheludkevich, S. K. Poznyak, L. M. Rodrigues, D. Raps, T. Hack, L. F. Dick, T. Nunes and M. G. S. Ferreira, *Corros. Sci.,* 2010, **52**, 602-611.
8. M. Kendig, M. Hon and L. Warren, *Prog. Org.Coat.*, 2003, **47**, 183-189.

9. J. Molina, M. F. Esteves, J. Fernández, J. Bonastre and F. Cases, *Eur. Polym. J.*, 2011, **47**, 2003-2015.
10. N. K. Rawat, A. Ghosal and S. Ahmad, *RSC Advances*, 2014, **4**, 50594-50605.
11. R. Jadhav, D. Hundiwale and P. Mahulikar, *J. Coat. Technol. Res.*, 2010, **7**, 449-454.
12. Y. Jafari, M. Shabani-Nooshabadi and S. M. Ghoreishi, *Polym. Adv. Technol.*, 2014, **25**, 279-287.
13. S. S. Jeon, S. J. Yang, K.-J. Lee and S. S. Im, *Polymer.*, 2010, **51**, 4069-4076.
14. S. Bhadra, D. Khastgir, N. K. Singha and J. H. Lee, *Prog. Polym. Sci.*, 2009, **34**, 783-810.
15. P. M. McManus, R. J. Cushman and S. C. Yang, *J. Phys. Chem.*, 1987, **91**, 744-747.
16. B. Belaabed, S. Lamouri, N. Naar, P. Bourson and S. Ould Saad Hamady, *Polym. J.*, 2010, **42**, 546-554.
17. S. Palaniappan and A. John, *Prog. Polym. Sci.*, 2008, **33**, 732-758.
18. H. Wei, D. Ding, S. Wei and Z. Guo, *J. Mat. Chem A.*, 2013, **1**, 10805-10813.
19. F. Chen and P. Liu, *ACS Appl Mater Inte.*, 2011, **3**, 2694-2702.
20. P. Fu, H. Li, J. Sun, Z. Yi and G.-c. Wang, *Prog. Org. Coat.*, 2013, **76**, 589-595.
21. P. A. Kilmartin, L. Trier and G. A. Wright, *Synthetic Met.*, 2002, **131**, 99-109.
22. P. J. Kinlen, D. C. Silverman and C. R. Jeffreys, *Synthetic Met.*, 1997, **85**, 1327-1332.
23. T. D. Nguyen, T. A. Nguyen, M. C. Pham, B. Piro, B. Normand and H. Takenouti, *J. Electroanal Chem.*, 2004, **572**, 225-234.
24. S. Radhakrishnan, C. R. Siju, D. Mahanta, S. Patil and G. Madras, *Electrochim Acta.*, 2009, **54**, 1249-1254.
25. S. Sathiyanarayanan, S. Muthkrishnan and G. Venkatachari, *Electrochim Acta.*, 2006, **51**, 6313-6319.
26. S. AHMAD, S. Ashraf and A. HASNAT, *Paintindia*, 2002, **52**, 47-52.
27. S. Ahmad, A. Gupta, E. Sharmin, M. Alam and S. Pandey, *Prog. Org.Coat.*, 2005, **54**, 248-255.
28. S. Ahmad, U. Riaz, M. Kashif and M. Khan, *J. Inorg. Organomet. Polym.*, 2012, **22**, 662-670.
29. S. Ashraf, S. Ahmad, U. Riaz, M. Alam and H. Sharma, *J. Macromol. Sci A.*, 2005, **42**, 1409-1421.
30. C. M. Chang and J. M. Yeh, *Adv Mat Res.*, 2013, **747**, 35-38.
31. Y. Chen, X. H. Wang, J. Li, J. L. Lu and F. S. Wang, *Corros Sci.*, 2007, **49**, 3052-3063.
32. C. Damian, A. Pandele, C. Andronescu, A. Ghebaur, S. Garea and H. Iovu, *Fuller. Nanotub. Car. N.*, 2011, **19**, 197-209.
33. S. Dutta, N. Karak, J. P. Saikia and B. K. Konwar, *Bioresour. Technol.*, 2009, **100**, 6391-6397.
34. L. Esposito, J. Ramos and G. Kortaberria, *Prog. Org.Coat.*, 2014, **77**, 1452-1458.
35. K. Gaw and M. Kakimoto, in *Progress in Polyimide Chemistry I*, Springer, 1999, pp. 107-136.
36. Y. Guo, C. Bao, L. Song, B. Yuan and Y. Hu, *Ind. Eng. Chem. Res.*, 2011, **50**, 7772-7783.
37. T. Iijima, N. Yoshioka and M. Tomoi, *Eur. Polym. J.,* 1992, **28**, 573-581.
38. A. Gök, M. Omastová and A. G. Yavuz, *Synthetic. Met.*, 2007, **157**, 23-29.
39. M. Mobin and N. Tanveer, *J. Coat. Technol. Res.*, 2012, **9**, 27-38.
40. N. Tanveer and M. Mobin, *JMMCE*, 2011, **10**, 735.
41. B.-J. Kim, S.-G. Oh, M.-G. Han and S.-S. Im, *Synthetic. Met.*, 2001, **122**, 297-304.
42. S. Ahmad, U. Riaz, A. Kaushik and J. Alam, *J. Inorg. Organomet. Polym.*, 2009, **19**, 355-360.
43. S. J. Lee, J. M. Lee, I. W. Cheong, H. Lee and J. H. Kim, *J. Polym. Sci. A. Polym.*, 2008, **46**, 2097-2107.
44. A. C. C. de Leon, R. B. Pernites and R. C. Advincula, *ACS Appl Mater Interfaces.*, 2012, **4**, 3169-3176.
45. T. P. Chou, C. Chandrasekaran, S. J. Limmer, S. Seraji, Y. Wu, M. J. Forbess, C. Nguyen and G. Z. Cao, *J. Non-Cryst. S.*, 2001, **290**, 153-162.
46. N. Pirhady Tavandashti, S. Sanjabi and T. Shahrabi, *Prog. Org. Coat.*, 2009, **65**, 182-186.

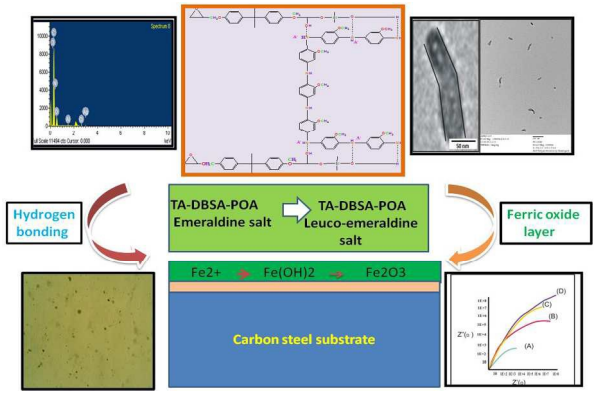

Tartaric acid- dodecylbenzenesulphonic acid doped Poly(o-anisidine) dispersed epoxy-siloxane nanocomposites have exhibited a promising application as new generation smart anti-corrosive coating materials